Supplementary Material for: Like-charge interactions between colloidal particles are asymmetric with respect to sign

Esther W. Gomez[1,4], Nathan G. Clack[3], Hung-Jen Wu[4], and Jay T. Groves[2,4,5,6]

Departments of Chemical Engineering[1] and Chemistry[2] and Biophysics[3] Graduate Group, University of California, Berkeley, CA 94720
Physical Biosciences[4] and Materials Sciences[5] Divisions, Lawrence Berkeley National Laboratory, Berkeley, CA 94720
Howard Hughes Medical Institute[6], Chevy Chase, MD

To whom correspondence should be addressed: J.T.G. (JTGroves@lbl.gov)

Contents

Supplementary Discussion

Radial distribution function analysis

Average radial distribution functions, *g(r)*, were calculated from a collection of brightfield images acquired at different locations in the same sample such that recorded configurations were non-overlapping. Center-to-center particle pair distances were measured to compute *g(r)* for individual images as previously described [1,2]. The average *g(r)* was calculated using aggregate pair distances from the full data set with a bin size of 50 nm.

Individual particles were located laterally by applying a threshold, yielding pixel-precision estimates of particle location. The location of particles was then refined by isolating individual particle images, bicubically interpolating to subpixel precision, and locating the maximal intensity on the interpolated image. The resolution of this method was estimated computationally by perturbing experimental images with additive zero-mean gaussian noise with variance estimated from the background. Results suggest a resolution of approximately 25 nm.

For samples in which particles are in close proximity to each other the image from an individual particle can extend beyond the hard-sphere diameter of the particle affecting the image of nearby neighbors. This introduces a systematic error in estimated center-to-center distances. Assuming the scattering from nearby particles is additive, the magnitude of this error may be estimated computationally, by juxtaposing two identical images of a single isolated particle a known distance apart and measuring the apparent center-to-center distance [3]. This is repeated for 100 particle images to calculate the average correction. The magnitude of the correction can differ from data set to data set due to variation in focus or illumination, but typically corrections are less than 100 nm. Corrections larger than the estimated lateral resolution are required for pairs within 50 nm of hard sphere contact. However, for the experiments here, few particle pairs were observed in this region. Nonetheless, the correction was applied to all measured center-to-center distances.

When computing the degree of local ordering, *G*, as defined in equation 1 of the main text we use r_o = mean bead diameter and r_1 = 8.45 μm. We chose r_1 to be the average distance at which the *g(r)* function first falls below a value of 1 (between the first and second peaks) for samples that condense strongly (negative Ψ). For consistency, r_1 is kept constant throughout the analysis.

Dual wavelength reflection interference contrast microscopy analysis

During RICM imaging, each particle generates a wavelength-dependent interferogram that is independent from neighboring particles. In this work, the sample is illuminated with two color bands: blue (460-480 nm) and green (520-550 nm). An image splitting device separates the reflected light according to wavelength and projects the corresponding interferograms for simultaneous imaging onto separate halves of a charge-coupled device (CCD) camera.

Heights of individual particles were determined from dual wavelength RICM micrographs using an image correlation technique as previously described [4]. Interferogram pairs corresponding to a single particle are analyzed to determine the height of the particle by correlating the image from

each channel with calculated interferograms. The particle height is determined by finding the pair of local correlation maxima that coincide across each channel. Lateral positions are measured independently in each channel by image correlation. Images where there is no unique agreement correspond to malformed or partially imaged particles and were excluded from further analysis.

Calculations suggest that using this dual wavelength RICM configuration, heights can be measured over a 2 μm absolute range. Experimentally, the absolute range is shorter since interference contrast decreases at higher particle heights and begins to compete with noise. This effect is estimated computationally by adding white noise (mean and variance estimated from the background in experimental data) to simulated data sets. Based on these results, image processing reliably estimates particle height from 0 to 1300 nm. Here, observed particle heights range between 0 nm and 800 nm. This maximal height corresponds with that expected for very highly charged 6.54 μm diameter particles. Hence, we expect reported heights are accurate.

Surface potential calculation

Equilibrium particle heights were used to calculate the particle surface potentials using the Poisson-Boltzmann equation as described below [5-7].

The potential energy profile for a particle levitated above a like-charged wall can be calculated by summing the electrostatic, gravitational, and dispersion forces acting on the system. For large particle-wall separations, dispersion forces are negligible compared to gravity and double layer repulsion and the potential energy is given by

$$\phi(h) = \phi_{edl}(h) + \phi_{grav}(h) \qquad \text{(S1)}$$

where $\phi_{edl}(h)$ is the electrostatic double layer repulsion and $\phi_{grav}(h)$ is the gravitational contribution for a given height, h. When the particle wall separation is large compared to the Debye length and the particle is suspended in a solution of 1:1 electrolyte ($\kappa h > 1$), the electrostatic double layer term can be computed using the superposition and Derjaguin approximations and is given by the following

$$\begin{aligned} \phi_{edl}(h) &= B\exp(-\kappa h) \\ B &= 64\pi\varepsilon a\left(\frac{k_B T}{e}\right)^2 \tanh\left(\frac{e\Psi_p}{4k_B T}\right)\tanh\left(\frac{e\Psi_w}{4k_B T}\right) \\ \kappa &= \left(\frac{2CN_A e^2}{\varepsilon k_B T}\right)^{0.5} \end{aligned} \qquad \text{(S2)}$$

where κ^{-1} is the Debye length, ε is the dielectric permittivity of water, a is the particle radius, k_B is the Boltzmann constant, T is the temperature, e is the charge of an electron, Ψ_p and Ψ_w are the particle and wall surface potentials respectively, C is the electrolyte concentration, and

N_A is Avogadro's number. When both the particle and the wall are coated with membranes of the same composition $\Psi_p = \Psi_w = \Psi$ and equation S2 can be expressed as

$$B = 64\pi\varepsilon a\left(\frac{k_B T}{e}\right)^2 \tanh^2\left(\frac{e\Psi}{4k_B T}\right). \qquad \text{(S3)}$$

The gravitational potential energy is given by

$$\phi_{grav}(h) = mgh = (4/3)\pi a^3\left(\rho_p - \rho_f\right)gh \qquad \text{(S4)}$$

where *m* is the mass of the particle, *g* is the gravitational constant, ρ_p is the particle density, and ρ_f is the density of the fluid.

The minimum potential energy occurs when the particle is levitated at an equilibrium height h_m above the underlying substrate. Solving for h_m gives

$$\kappa h_m = \ln\left(\kappa B/mg\right) \qquad \text{(S5)}$$

Combining equations S1-S5 allows for one to solve for the particle and wall surface potential, Ψ.

For a sphere, the surface charge density, *q*, can then be calculated from the surface potential using the following equation[5]

$$q = \frac{\varepsilon\varepsilon_o kT}{ez}\kappa\left[2\sinh\left(\frac{ez\Psi}{2kT}\right) + \frac{4}{\kappa a}\tanh\left(\frac{ez\Psi}{4kT}\right)\right] \qquad \text{(S6)}$$

Equation S6 is valid for $\kappa a > 0.5$.

Although the choice of an alternate model may yield more accurate computed surface potentials, it is important to note that the membrane-coated particle systems explored are matched based on physical repulsion from the underlying substrate with the relevant measured parameter being the equivalent heights of particles above the underlying substrate for oppositely charged systems. Thus, the systems can be matched in a model independent manner and the choice of surface potential model does not change the overall interpretation of the results.

Surface potentials reported in Figure 2c for bare silica and amine-functionalized silica experiments were computed assuming $\Psi_p = \Psi_w$. This assumption does not take into account differences in the surface chemistries of silica and borosilicate glass; however, this not change the overall conclusions given that silica particles and borosilicate glass are both negatively charged and the particles are observed to form crystallites at low surface densities.

Ergodicity

Membrane-coated particles settle, gravitationally, to an equilibrium height above a like-charged underlying planar supported bilayer within 5 minutes of being cast into a well plate. The particles are free to diffuse in two dimensions by Brownian motion. Although the particles continue to move and the system evolves through different microscopic configurations, the distribution remains constant during the experimental time frame as shown in Fig. S1.

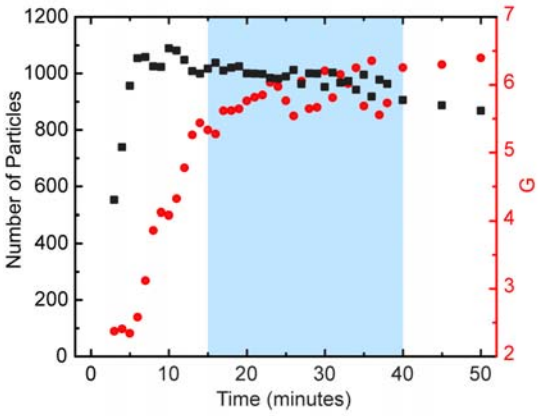

Fig. S1. Time sequence of colloidal distribution. Particles coated with negatively charged membranes (Ψ ~ -55 mV) condense into hexagonally packed crystallites over time. The number of particles (black squares) and the local order, quantified in terms of *G* (red circles), remain stable over the experimental time frame (shaded blue region).

The heights of the membrane coated particles are monitored *in situ* by dual wavelength reflection interference contrast microscopy (RICM). During the experimental time frame the heights fluctuate about an equilibrium height as shown in Fig. S2.

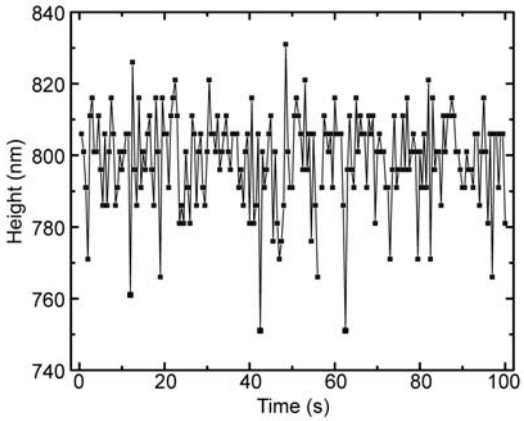

Fig. S2. Height time sequence for a single particle. The height of a membrane coated particle (Ψ = - 53 mV) fluctuates about a mean height.

Ergodicity of the colloidal distributions is illustrated by their rapid response to changes in surface properties of the particles [1] and changes in bulk fluid properties. Changing the ionic strength of the bulk solution for a negatively charged system (Ψ ~ - 55 mV) results in a change from strongly condensed to dispersed as shown in Fig. S3. The long-range attractive interaction between the particles is screened by the addition of salt resulting in the dissolution of the crystallites.

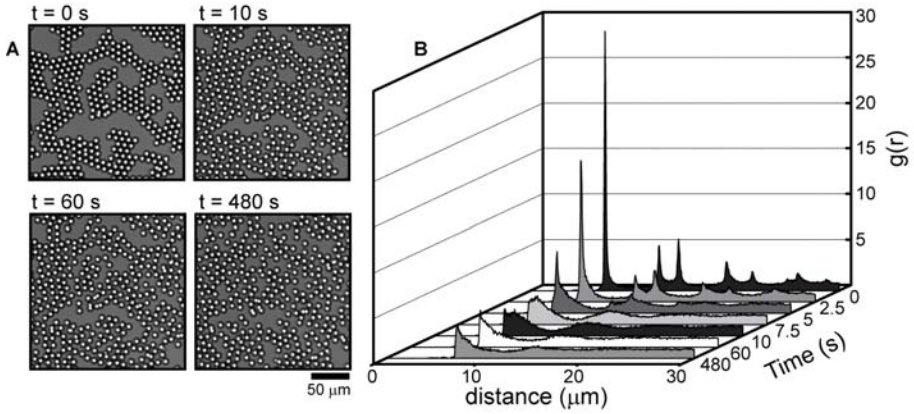

Fig. S3. Colloidal distributions have a rapid response to changes in bulk fluid properties. (A) Time sequence of brightfield images for particles coated with negatively charged membranes (Ψ ~ - 55 mV) illustrates the change in colloidal ordering upon addition of NaCl. The ionic strength is adjusted by adding 50 mM NaCl (to a final concentration of 260 μM) at t = 0 seconds and within 10 seconds the particles begin to disperse. (B) Corresponding *g(r)* plots.

Particle surface control and characterization

Lipid membrane coatings were used to control the surface chemistry of particles and substrates. Membrane composition and the resulting surface potential were varied by incorporating differing amounts of lipids with acidic and basic headgroups. Particle surface potential was monitored *in situ* using dual wavelength reflection interference contrast microscopy (RICM). Heights of particles levitated above a like-charged substrate for various membrane coatings obtained from dual wavelength RICM experiments are shown in Fig. S4(A). The height increases with increasing charge density and is symmetric about the point of zero charge. The corresponding surface potential, Ψ, which was computed using the Poisson-Boltzmann theory as outlined in the Discussion section above, is plotted in Fig. S4(B) and surface charge density in Figure S4(C). The sign of the particle surface potential was confirmed by observing membrane coated particles over positively and negatively charged substrates. Particles with surface charges of the same sign as the underlying substrate were mobile while particles of opposite sign were immobile. Systems can be matched electrostatically such that the magnitude of the surface potentials are equal but opposite in sign.

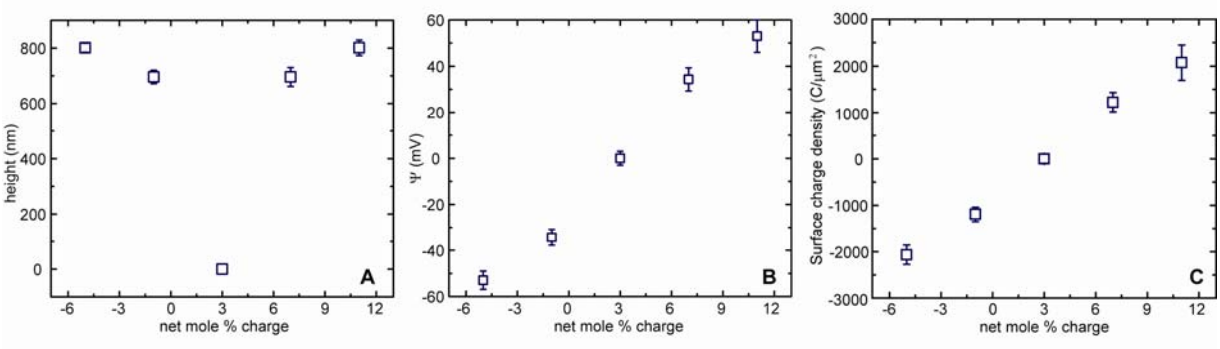

Fig. S4. Dual wavelength RICM results for various membrane compositions. (A) Experimental heights for particles coated with membranes of various charge densities obtained from analysis of dual wavelength RICM interferograms. Corresponding surface potentials (B) and surface charge densities (C) computed from equations outlined in surface potential calculation section of Supplementary Material.

Ionic strength

The effect of electrolyte concentration and composition on colloidal ordering was studied. The local order, *G*, as a function of ionic strength is plotted in Figure 3B of the main text and corresponding values of *G* are given in Table S1 below for $\Psi \sim \pm 55$ mV. The values of *G* are reproducible from day to day.

Table S1. Effect of monovalent salt species on the local ordering of two dimensional dispersions of membrane-coated particles expressed in terms of *G*.

Ionic Strength (μM)	Positive Membrane				Negative Membrane			
	NaCl	$N(CH_3)_4Cl$	NH_4Cl	$NaCH_3COO$	NaCl	$N(CH_3)_4Cl$	NH_4Cl	$NaCH_3COO$
10	0.9	1.0	1.0	0.8	6.7	5.2	5.4	5.6, 5.6
40	1.0	1.4	1.4	1.5	4.1	3.7	3.5	3.0, 2.9
70	1.3	1.2	1.2	1.3	3.4	2.6	2.9	2.4, 2.5
135	1.9	1.3	1.3	1.8	2.4	1.9	2.2	1.9, 1.9
260	1.4	1.8	1.8	1.6	1.8	1.7	1.8	1.7, 1.7
510	1.5	1.5	1.5	1.7	1.5	1.5	1.8	1.7, 1.6

To test whether the repulsive component of the colloid interaction potential is well described by a pair-wise Poisson-Boltzmann interaction Monte Carlo simulations were performed for $\Psi = \pm$ 55 mV and a variety of ionic strengths. For comparison purposes the effective particle diameter was defined as the distance at which the first peak of *g(r)* attains its half maximal value. As the ionic strength increases the effective particle diameter decreases. The experimental effective particle diameter at various ionic strengths compares well to Monte Carlo results, as shown in Fig. S5. The error bars denote the resolution of our calculated *g(r)*, which is 50 nm.

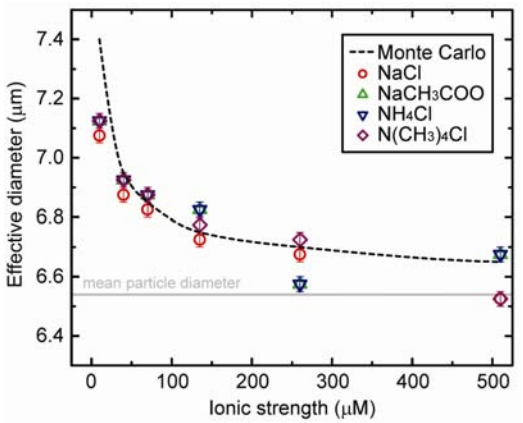

Fig. S5. Effective diameter of negatively charged particles (Ψ ~ - 55 mV) over a range of ionic strengths and electrolyte compositions.

Ion exchange resin was used to further deplete ions from the bulk solution, but our *in situ* electrostatic measurements suggest this is not particularly effective at ultra low ionic strengths in our experimental configuration. Thus, there is likely an unavoidable background of several micromolar carbonate in the water which will enhance the ionic asymmetry of the water. Importantly, this will be the case for essentially all experiments done in low ionic strength water in earth's atmosphere.

Membrane-coating characterization

A small amount of the fluorescently labeled lipid Texas red DPPE was incorporated into membranes to facilitate viewing of the membrane coating on particle and substrate surfaces. Membrane coatings were uniform when observed by fluorescence microscopy as shown in Fig. 1c (of the main text) and Fig. S6, suggesting homogeneity on the >200 nm length scale.

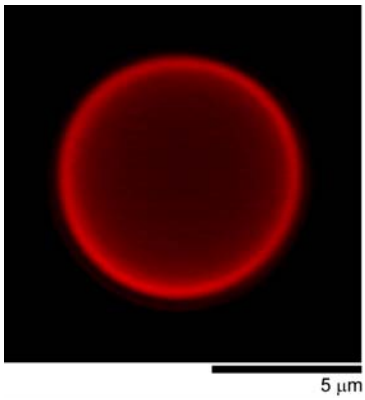

Fig S6. Fluorescence microscopy image of a membrane coated particle.

Analysis of depletion effects

We observe that bare silica particles form crystalline domains, ruling out lipid vesicles in solution as a possible source of depletant. Likewise, in scanning electron microscope (SEM)

images (Fig. S7), silica particles are uniform in size and fairly smooth suggesting that smaller silica particles are not present. To ensure that the particle solutions were free of any possible depletants, silica particles were cleaned thoroughly by gently and uniformly dispersing the particles in water overnight using a rotator followed by sedimentation through a 20 cm column. The silica particles cleaned using this procedure show no crystal structure (G=0.93) and upon addition of smaller silica particles (30, 50, and 200 nm silica particles, Kisker, Germany) to the solution to induce depletion interactions, the silica particles still do not form crystalline domains. Upon washing with base (0.1 N NaOH) the particles once again form crystalline domains, suggesting the observed attractive force may be associated with surface characteristics of the particles. There is no direct evidence of depletant in the solution.

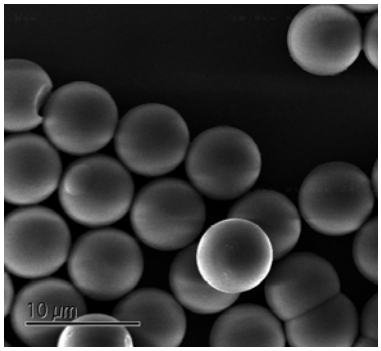

Fig. S7. SEM image of silica particles.

Polymer induced interactions

Condensation of like-charged colloids into structures resembling those observed here is commonly induced by addition of non-adsorbing polymers or smaller particles. When the distance between the surfaces of the larger particles becomes less than the diameter of the smaller particles, the smaller particles are excluded from the region between the larger particles. An osmotic pressure difference develops between the bulk solution and the region between the large particles resulting in an attractive entropic depletion force between the larger objects. For polyelectrolytes in solution, the magnitude and range of the depletion force can be largely increased [8-11]. However, the magnitude of depletion forces tends to be small. Likewise, depletion forces are typically only measured up to a separation distance of ~ 150 nm [9]. For the system studied here, particle surfaces are separated by ~ 1 μm in the highly condensed hexagonally packed crystallites.

To test whether non-adsorbing polymers can induce condensation between repulsive particles neutral polyethylene glycol (PEG) and positively charged poly (allylamine) hydrochloride (PAH) polymers were added to positively charged particles (Ψ ~ + 55 mV) suspended above a like-charged substrate. Addition of 1000 μg/mL (1000 ppm) PEG and PAH failed to induce condensation as shown in Fig. S8, suggesting that trace amounts of contaminants are not responsible for the condensation of negatively charged particles.

To investigate whether adsorbing polymers can induce condensation in a system that strictly repels, negatively charged polymer poly (sodium 4-styrene sulfonate) (PSS) was added to positively charged particles. Addition of ~ 1 μg/mL (1 ppm) of PSS resulted in condensation of

the membrane coated particles into hexagonally packed crystallites (Fig. S8). The sign of the particle surface charge after addition of PSS was confirmed by monitoring the mobility of the particles above positively and negatively charged substrates. Particles were only mobile over negatively charged substrates suggesting that the negatively charged PSS adsorbs to the surface of positively charged membrane coated particles, thereby changing their net charge to negative. Therefore, the observed condensation with the addition of PSS to positively charged particles is likely due to charge reversal of the membrane coated surfaces. At higher concentrations of PSS (1000 μg/mL) we observe a peak emerge at the particle diameter, r_o, rather than at ~ r_o + 1 μm. The membranes surfaces may be saturated with PSS, likely resulting in some soluble PSS in solution. Particle surfaces are in closer proximity which is likely a result of increased depletion interactions due to the unadsorbed PSS in solution.

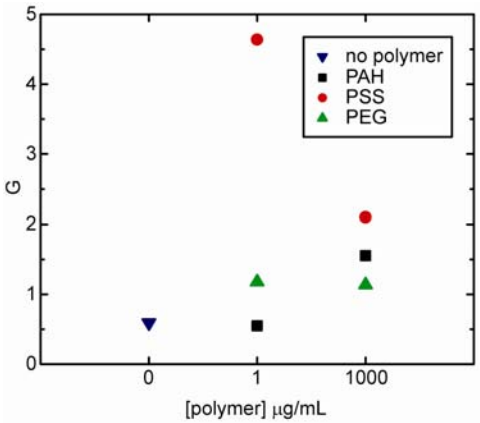

Fig. S8. Degree of local ordering, *G*, in positively charged membrane coated system (Ψ ~ + 55 mV) with addition of a variety of charged polymer species. Addition of positively charged PAH and neutral PEG results in small changes in the local order. Condensation of particles into hexagonally packed crystallites is only observed for addition of negatively charged PSS.

Addition of monovalent salt to the positively charged system that was incubated with PSS resulted in a reduction in the condensation between the particles (Fig. S9). This result is consistent with ionic strength results for negatively charged membrane coated particles and is further support of asymmetry with respect to the sign of the charge.

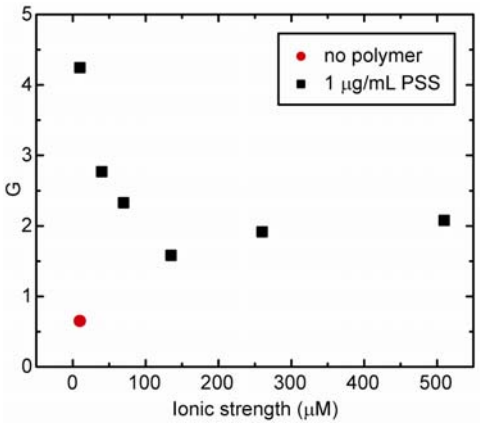

Fig. S9. Degree of local ordering, *G*, in positive surface potential system ($\Psi \sim +55$ mV) with addition of 1 μg/mL PSS as a function of ionic strength. The local order decreases with an increase in the concentration of the monovalent salt NaCl.

Factors that can influence measured interactions in colloidal systems

Imaging artifacts. Imaging artifacts that displace the apparent centroids of particles can result in erroneously determined particle positions which can create the appearance of an attractive pair potential when none exists [3]. For the system studied here, such artifacts are observable, and they are corrected for when computing particle center-to-center distances that are used to calculate *g(r)* functions. However, due to the large interparticle spacings, the correction has a very small affect on *g(r)*.

Convection. Fluid flow can lead to non-equilibrium forces that bring particles together. Local heating by illumination can result in convective flow within a sample which results in condensation and aggregation of particles [12]. In the experiments described here, the illumination power is low therefore local heating is minimal. Likewise, the different behavior observed between positively and negatively charged particles is not expected to result from convection.

Particle polydispersity. Particle polydispersity has also been proposed to contribute to observed apparent like-charge attractions [13]. For the experiments described here, samples of silica particles were taken from the same well-mixed stock population and are expected to have nearly equivalent polydispersities.

Multibody interactions. For particle surface area densities used here many body effects contribute to the colloidal behavior through crowding and non-additive interparticle potentials. Recent studies have shown that three-body potentials between like-charged particles can be attractive thus resulting in a reduction in the net repulsion between particles [14]. Due to the high particle surface density and experimental geometry used, we do not directly probe the pair potential between particles; however, we do observe differences in the net interaction over multiple particles for the cases of oppositely charged particles, which is anomalous as it is not predicted by current theories.

References

[1] Baksh, M. M., Jaros, M. & Groves, J. T. Detection of molecular interactions at membrane surfaces through colloid phase transitions. *Nature* **427**, 139-141 (2004).

[2] Winter, E. M. & Groves, J. T. Surface binding affinity measurements from order transitions of lipid membrane-coated colloidal particles. *Anal. Chem.* **78**, 174-180 (2006).

[3] Baumgartl, J. & Bechinger, C. On the limits of digital video microscopy. *Europhys. Lett.* **71**, 487-493 (2005).

[4] Clack, N. G. & Groves, J. T. Many-particle tracking with nanometer resolution in three dimensions by reflection interference contrast microscopy. *Langmuir* **21**, 6430-6435 (2005).

[5] Russel, W. B., Saville, D. A. & Schowalter, W. R. *Colloidal dispersions*. (Cambridge University Press, 1989).

[6] Frej, N. A. & Prieve, D. C. Hindered diffusion of a single sphere very near a wall in a nonuniform force-field. *J. Chem. Phys.* **98**, 7552-7564 (1993).

[7] Wu, H. J. & Bevan, M. A. Direct measurement of single and ensemble average particle-surface potential energy profiles. *Langmuir* **21**, 1244-1254 (2005).

[8] Walz, J. Y. & Sharma, A. Effect of long-range interactions on the depletion force between colloidal particles. *J. Colloid Interface Sci.* **168**, 485-496 (1994).

[9] Pagac, E. S., Tilton, R. D. & Prieve, D. C. Depletion attraction caused by unadsorbed polyelectrolytes. *Langmuir* **14**, 5106-5112 (1998).

[10] Rudhardt, D., Bechinger, C. & Leiderer, P. Direct measurement of depletion potentials in mixtures of colloids and nonionic polymers. *Phys. Rev. Lett.* **81**, 1330-1333 (1998).

[11] Biggs, S., Burns, J. L., Yan, Y. D., Jameson, G. J. & Jenkins, P. Molecular weight dependence of the depletion interaction between silica surfaces in solutions of sodium poly(styrene sulfonate). *Langmuir* **16**, 9242-9248 (2000).

[12] Garcés-Chavéz, V. *et al.* Extended organization of colloidal microparticles by surface plasmon polariton excitation. *Phys. Rev. B* **73**, 085417 (2006).

[13] Pangburn, T. O. & Bevan, M. A. Role of polydispersity in anomalous interactions in electrostatically levitated colloidal systems. *J. Chem. Phys.* **123**, 174904 (2005).

[14] Dobnikar, J., Brunner, M., von Grunberg, H. H. & Bechinger, C. Three-body interactions in colloidal systems. *Phys. Rev. E* **69**, 031402 (2004).